Phonon-assisted radiative recombination of excitons confined in strongly anisotropic nanostructures

Ł. Dusanowski,[1,*] A. Musiał,[1,†] A. Maryński,[1] P. Mrowiński,[1] J. Andrzejewski,[1] P. Machnikowski,[1] J. Misiewicz,[1] A. Somers,[2] S. Höfling,[2,‡] J. P. Reithmaier,[2,§] and G. Sęk[1]

[1]*Institute of Physics, Wrocław University of Technology, Wybrzeże Wyspiańskiego 27, 50-370 Wrocław, Poland*

[2]*Technische Physik, University of Würzburg and Wilhelm-Conrad-Röntgen-Research Center for Complex Material Systems (RCCM), Am Hubland, D-97074 Würzburg, Germany*

(Received 10 April 2014; revised manuscript received 25 July 2014; published 15 September 2014)

The influence of acoustic phonons on the emission spectra of quantum dashes (QDashes), that are quasi-zero-dimensional epitaxial nanostructures with significant shape anisotropy, is investigated both experimentally and theoretically. Photoluminescence (PL) spectra of single InAs/InGaAlAs/InP (001) QDashes exhibit sidebands of the main emission peak, clearly indicating the contribution of phonon-assisted emission to the exciton luminescence, which dominates the PL line shape at higher temperatures (between 50 and 100 K, usually). By utilizing the independent boson model we perform systematic and comprehensive studies of the influence of the overall geometry of quantum confinement on this spectral feature in an uncommon quantum system. A comparison of the experimental data and the results of modeling have confirmed the existence of two types of states differing in the spatial confinement and symmetry within one sample, i.e., typical for large elongated objects or characteristic for smaller and more symmetric structures. The latter are supposed to correspond to local widenings or zigzag bends present in some of the dashes and acting as additional localization centers, which confine excitons in a much smaller volume and decrease effectively the resulting in-plane anisotropy. Those observations evidence a nontrivial spatial character of the quantum confinement in these structures. They are consistent with our previous polarization-resolved study on the QDash ensemble and correlate well with the exciton decay times, and the spectral-diffusion-dominated line broadenings at low temperatures reflecting the effect of electric field fluctuations on the excitons of a different spatial extension. Finally, we demonstrate a pronounced suppression of phonon-induced decoherence for such strongly elongated nanostructures.

DOI: 10.1103/PhysRevB.90.125424 PACS number(s): 78.67.Hc, 63.20.kk

I. INTRODUCTION

Semiconductor quantum dashes (QDashes) are self-assembled nanostructures similar to quantum dots (QDs), however strongly elongated in one of the in-plane directions [1–8]. The majority of the reports regarding such strongly asymmetric objects concern the InAs-InP (001) material system, where elongation can easily be achieved spontaneously during the growth by molecular beam epitaxy [2–5]. The primary motivation to fabricate and study this type of structures was their proven application potential in optoelectronics. InAs dashes on InP can emit light in the telecommunication window around 1.55 μm which, combined with unique properties of artificial-atom-like structures, very high surface density, broad gain function, and nearly instantaneous gain response, all providing extraordinary spectral tunability and high-speed modulation, makes them favorable as an active medium in lasers and optical amplifiers [9–12]. The laser-related properties of the QDash ensemble have already been extensively investigated and many details have been understood and reported, as for instance the influence of the growth parameters on the nanostructure geometry, QDash ensemble homogeneity and emission energy, as well as the electronic structure [9,13–15]. In addition, polarization properties of emission along with the spatial character and strength of the quantum confinement have also been studied [16,17]. In contrast, only a few theoretical and experimental reports have been published to date concerning the optical properties of single InAs/InP (001) QDashes focusing mainly on the exciton-biexciton cascade and its characteristics [18–25]. Because of the enlarged size and strong in-plane elongation of those structures, their optical properties are difficult to infer from the experiments and calculations performed for more common and almost symmetric objects. Neither experimental nor theoretical reports regarding the analysis of the influence of the exciton-phonon interaction on the emission spectra of anisotropic dashlike nanostructures are available. InAs/InP QDashes can be especially interesting in that respect due to the possible coexistence of two types of states differing intrinsically in the confinement regime, predicted previously based on polarization-dependent studies of the emission from QDash ensembles [26]. Local widenings, zigzag corners, and other shape or composition fluctuations within a quantum dash act as an additional localization center so that the exciton can be confined in a much smaller and less anisotropic space than in the case of a regular dash where the wave function is delocalized over the entire nanostructure volume [25,26]. These two types of objects: (i) with a localization center resembling symmetric QDs and (ii) without a localization center, i.e., uniform, strongly anisotropic nanostructures, are expected to differ with respect to interaction with phonons, which can be investigated via the visibility of the phonon-related spectral features [27], which

*Corresponding author: lukasz.dusanowski@pwr.edu.pl

†Currently at: Institut für Festkörperphysik, Technische Universität Berlin, Hardenbergstraße 36, D-10623 Berlin, Germany.

‡Currently at: School of Physics and Astronomy, University of St. Andrews, North Haugh, KY16 9SS, United Kingdom.

§Currently at: Institute of Nanostructure Technologies and Analytics (INA), CINSaT, University of Kassel, Heinrich-Plett-Strasse 40, 34132 Kassel, Germany.

are confinement dependent. So far no watertight experimental evidence of the existence of the two types of states nor a clear distinction between them, indispensable for more detailed study, have been reported for individual QDashes.

Another feature making QDashes very interesting in view of both fundamental research and applications is the confinement regime. Domination of the spatial confinement effects (strong confinement regime) is expected for nanostructures where: (i) the quantization energy is much larger than the exciton binding energy, i.e., the energy scale characteristic for Coulomb interactions between the carriers confined in a quantum dot, and (ii) the volume of the exciton (defined by the exciton Bohr radius) is larger than the physical volume of the nanostructure. In the case of weak confinement regime, the Coulomb interactions start to prevail over the quantum confinement effects on the single carriers. In this regime, the oscillator strength of optical transitions is governed mainly by the exciton coherence volume which increases with the QD size. QDashes seem to belong to an intermediate regime [17], and depending on their size can be tuned between the two ultimate cases. This results from a combination of their small cross-sectional size with pronounced elongation leading to an enlarged nanostructure volume compared to more common symmetric self-assembled quantum dots of the same material system. However, the exciton volume (exciton Bohr radius in InAs is more than 30 nm) is still slightly smaller than the physical volume of a quantum dash, but on the other hand, the energy level separation for electrons and holes is on the order of 30 meV for less anisotropic dashlike structures to significantly below 10 meV for more than 100 nm long quantum dashes [17]. Our previous study indicated that it might be possible to distinguish between the effect of the size in the cross-sectional/strongest confinement directions and the elongation direction on properties like Coulomb correlations or carrier kinetics [17,23]. Such unusual properties of the dashes make an unprecedented opportunity for the fundamental study of different effects individually, and allow for independent "tuning knobs" assuring additional flexibility required for some of the nanophotonic applications.

The interaction of an exciton with phonons can be manifested experimentally in the change of the line shape of the optical response (either absorption or emission). In the process of exciton generation or recombination accompanied by phonon absorption or emission, the photon energy is shifted by the energy of the involved phonons [28–30] and phonon sidebands are observed in the optical spectra [31]. In the case of emission lines, this effect has already been investigated experimentally in symmetric QDs, where by analyzing the exciton line shape at different temperatures a strong deviation from the expected Lorentzian profile has been observed expressed in the appearance of low-energy acoustic-phonon sidebands [31–34]. In general, it is expected that an exciton confined in a larger quantum object should exhibit a weaker interaction with phonons [31,32,34,35]. This is due to the wave vector cutoff, approximately at the inverse of the structure size. The number of phonon modes that can effectively couple to the exciton is reduced for larger nanostructures limiting the width of the phonon sidebands [30,36]. It has not been verified so far how this general rule is manifested in strongly anisotropic nanostructures, such as QDashes. In particular, the following issues are unexplored: (i) the importance of the shape asymmetry and the role of the confinement in different directions; (ii) the interplay between various carrier-phonon coupling mechanisms; and (iii) the possible effect of strain and Coulomb interactions. The existing reports are limited to the influence of the base size of QDs preserving the in-plane rotational symmetry and for nanostructures of smaller volume [27,31,34,36–38] than the ones considered here (by approximately one order of magnitude). QDashes combine enlarged volume and strong shape anisotropy, which makes them interesting from the point of view of phonon-assisted exciton recombination. Understanding of the physics governing this process is important not only for fundamental research, but it is also crucial for futuristic and sophisticated applications based on single quantum emitters, like single-photon sources or nanolasers. These are required to operate in the telecommunication spectral range [21,39,40] for which the InAs/InP nanostructures are perfectly well suited.

In this paper we investigate the phonon-assisted recombination process of excitons confined in InAs QDashes grown epitaxially on InP substrates. Our goal is to determine whether the increased size and the asymmetry of a quantum object makes these nanostructures more robust against the phonon-induced effects and hence the related exciton state decoherence. To this end, the temperature dependent linewidth of single QDash emission peaks observed in microphotoluminescence (μPL) experiment was measured and confronted with the results of theoretical modeling confirming the existence of two types of states of a different confinement. We investigated also which exciton-phonon coupling mechanism dominates the system properties and analyzed the changes of the exciton line broadening as a function of phonon mode occupations (temperature) for different QDash geometries and initial (low-temperature) inhomogeneous broadenings of the exciton peak mimicking the spectral diffusion effects.

The paper is organized as follows. In Sec. II the investigated structures and experimental setup are described. The results are discussed in the following Sec. III. First, there is presented an example of experimental results of temperature-dependent microphotoluminescence spectra with clearly resolved phonon-related features (Sec. III A). Then the theoretical approach is described (Sec. III B), followed by the results of simulations of the influence of geometry on the emission line shape (Sec. III C). And finally a direct comparison of the results of modeling and the measurements is made (Sec. III D). Section IV concludes the paper.

II. SAMPLES AND EXPERIMENTAL SETUP

The investigated structures are InAs quantum dashes grown by molecular beam epitaxy on InP (001) substrates. The QDash layer is surrounded by $In_{0.53}Ga_{0.23}Al_{0.24}As$ barriers, lattice matched to InP. Due to the diffusion coefficient anisotropy, the epitaxially formed nanostructures are significantly elongated in one of the in-plane directions (preferentially [1−10]). The lateral dimensions are approximately 10–25 nm nanometers in width and 50 up to several hundreds of nanometers in length. The height is typically on the order of a few nanometers. It has been shown that the cross-sectional dimensions of the QDash can be controlled in a wide range

by a single technological parameter—the nominal thickness of the deposited InAs material [4]. In this paper we focus on structures fabricated with a nominal thickness of 1.05 nm InAs. This leads to the formation of nanostructures with typically triangular or lens-shaped cross sections of the size $16 \times 3.0\,\mathrm{nm}^2$, and average length of the dashes equal to around 100 nm resulting in room temperature emission centered at 1.55 μm. The surface density of the dashes is very high, exceeding significantly $10^{10}\,\mathrm{cm}^{-2}$, therefore for single dash spectroscopy the sample was patterned with submicron-size mesas obtained by combining electron beam lithography and reactive ion etching. Some fundamental optical properties of the considered InAs/InGaAlAs/InP QDashes have already been investigated for single nanostructures [22–24] as well as for whole ensembles [26,41]. Among others, the problem of luminescence polarization was addressed in case of an ensemble of QDashes [27] where a nontrivial behavior of the temperature dependence of the degree of linear polarization was observed and modeled by assuming the existence of confinement potential fluctuations able to trap the excitons in a smaller volume of effectively lower asymmetry.

For the optical spectroscopy experiments the samples were kept in a liquid helium continuous-flow cryostat, which allows one to vary the temperature between 5 and 300 K. Microphotoluminescence (μPL) measurements were performed in a far field free space configuration using a microscope objective (NA = 0.4) giving a laser excitation spot size on the sample surface of about 2 μm (diffraction limit), providing high enough spatial resolution to investigate one mesa at a time. The samples were excited nonresonantly with the 660-nm line (1.88 eV) of a semiconductor continuous-wave laser. The emission intensity was detected by an enhanced sensitivity liquid-nitrogen-cooled InGaAs linear array detector combined with a 1.0 m focal length single-grating monochromator. The spectral resolution in this case was around 30 μeV. Good spectral separation of the emission lines has been obtained for $550 \times 275\,\mathrm{nm}^2$ sized mesas. In order to probe excitons only, and exclude other exciton complexes, the line identification was performed by power- and polarization-resolved μPL measurements [23,24]. Since most of the excitonic lines show a fine structure splitting on the order of 50 to 200 μeV, the temperature dependent emission spectra have been collected at selected linear polarization, so that only one split excitonic bright state was effectively detected. This has ensured that the exciton fine structure splitting causes no artificial emission line broadening. In addition, time-resolved photoluminescence experiments have been performed for the chosen lines, allowing determination of the characteristic decay times. Details of these studies can be found elsewhere [24].

III. RESULTS

A. Experimental observations

In Fig. 1 we present the μPL spectra of single InAs/InP QDashes with a nominal cross-sectional size of $16 \times 3\,\mathrm{nm}^2$ from $500 \times 275\,\mathrm{nm}^2$ mesa measured at temperatures from 5 up to 75 K. As can partly be seen in Fig. 1 (and also in the inset to Fig. 2), the low-temperature emission lines are influenced by spectral diffusion effects. Based on measurements performed

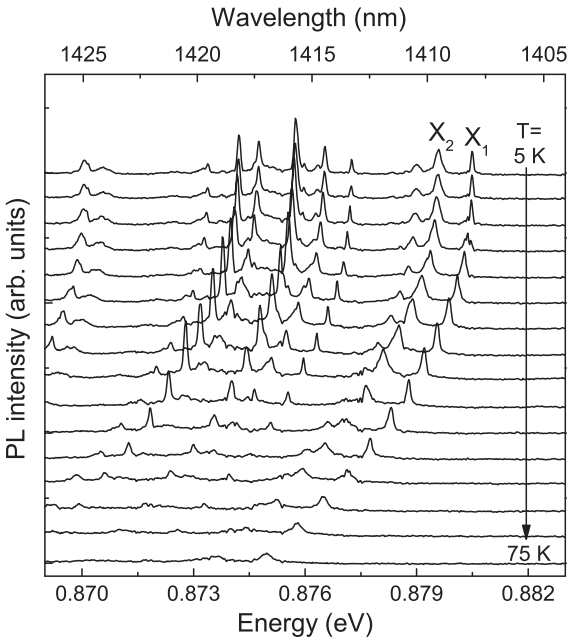

FIG. 1. Temperature dependence of the μPL spectra of single InAs/InP QDashes originating from the sample with a nominal dash size of $100 \times 20 \times 3.5\,\mathrm{nm}^3$ in the range of 5–90 K.

on several mesas and for many investigated dashes the low-temperature full widths at half maximum (FWHM) of the emission lines have been obtained to vary from dash to dash within a range of 0.1–0.2 meV. The recorded linewidths are almost two orders of magnitude larger than the lifetime-limited homogenous broadening corresponding to 1–2 ns exciton lifetime, typical for InAs/InP QDashes [17,24], and a few times larger than the instrumental resolution. Moreover, the PL peaks show a Gaussian line shape, indicating the inhomogeneous environmental impact on the quantum dash emission [42]. The spread of the low-temperature linewidths

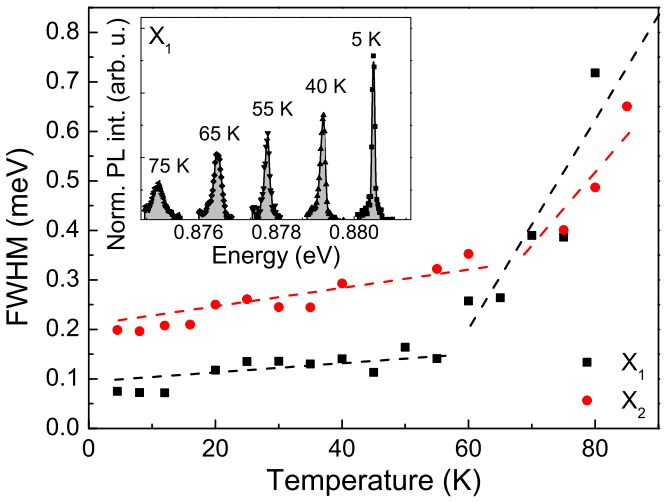

FIG. 2. (Color online) Temperature dependence of the FWHM of two representative lines from the spectra in Fig. 1. Dashed lines are a guide to the eye. Inset: μPL spectra of line 1 for selected temperatures, normalized to the integrated intensity.

can be explained by either various QDash positions with respect to the mesa sidewalls, where most of the possible carrier traps are located and form an important source of the local electric environment fluctuations or, more likely, by the QDash size distribution, which is effectively strongly enhanced due to the aforementioned effect of the additional trapping/localization centers within some of the dashes. The larger effective confining volume makes such excitons more vulnerable to quantum confined Stark effect [43], which leads to an enhancement of the linewidth in a fluctuating local field. As we show below, we can find evidence for the correlation between the linewidth and other confinement-related effects, which confirms the latter hypothesis.

As the temperature increases, the emission lines redshift and their intensity quenches. For all QDashes, the emission line shapes can be well characterized by a single Gaussian peak up to temperatures of 50–60 K, with a slight rise of its width (FWHM) with temperature. Above this temperature, sideband emission starts to be visible at the bottom of the single dash PL lines, and its contribution to the overall emission intensity rises abruptly with temperature. Above about 60–80 K the emission becomes dominated mainly by these sidebands. In order to perform a more quantitative analysis of the line shape changes with temperature, the FWHM is plotted as a function of temperature for two lines identified as excitons in two different dashes (marked as X_1 and X_2 in Fig. 1). Up to 40–50 K, the FWHM increases very slowly, then at temperatures exceeding around 60 K the increase becomes more abrupt. The analysis at temperatures above 90–100 K was usually not possible due to the thermal quenching and the drop of the signal to noise ratio below the detection limit.

The measurements have been performed on many other excitonic lines and actually all of them exhibit qualitatively similar line shape changes with temperature, differing only in the initial low-temperature broadening, slopes of the slow and fast FWHM buildups with temperature, and the critical "bending" temperature. Those differences are visible for lines X_1 and X_2 (Fig. 2). The observed line shape changes with temperature can be explained based on the effect of exciton coupling with acoustic phonons, manifested in the emission spectra as an appearance of phonon sidebands, which results from exciton recombination accompanied by a phonon absorption or emission, so that the photon energy is shifted by the energy of the involved phonons. More profound insight into the understanding of this phonon-assisted exciton recombination cannot be achieved without a theoretical modeling, which would allow us to evaluate the influence of parameters, crucial in the case of anisotropic objects, like size, geometry, or the wave-function (probability density distribution) symmetry. Analysis of the PL spectra for QDashes differing in geometry and initial low-temperature broadenings of exciton line will be presented in Sec. III D after describing the theoretical approach towards modeling the acoustic phonon-assisted exciton recombination in QDashes, followed by simulation results.

B. Theory

In order to reflect their significant anisotropy, the confining potential of QDashes is approximated by a wide and infinite barrier quantum well in the direction of the elongation, whereas the dynamics in the cross-sectional directions is restricted to the ground state and a two-dimensional (2D) harmonic potential is assumed. This model has been developed to study asymmetric nanostructures and it assumes that the electron and hole wave functions take a form of Gaussians (solutions of the 2D-harmonic oscillator) for the cross sectional directions, and the sine function (solution of an infinite quantum well) in the direction of the elongation. Distinction of the elongation axis, connected with the much weaker confinement direction, allowed us to restrict the dynamics to one dimension, which reduces the single particle basis and significantly simplifies calculations of the exciton states. This limits the applicability of the model to objects with at least some size anisotropy in the plane to fulfill the mentioned assumptions.

In that case, single-carrier, electron (e) and hole (h) states can be described by the wave functions

$$\psi_n^{(e/h)}(r) = \sqrt{\frac{2}{\pi l_z l_y l_x}} \exp\left(-\frac{y^2}{2l_y^2} - \frac{z^2}{2l_z^2}\right) \sin\left(\frac{n\pi x}{l_x}\right), \quad (1)$$

where l_y, l_z are localization widths in the cross section, l_x is the well width in the direction of the elongation, and n is the quantum number corresponding to the one-dimensional dynamics in the x direction. The parameters l_y, l_z, l_x are related to the QDash width D, height H, and length L. In order to get a better insight how the model parameters scale up with the real physical QDash dimensions and for the sake of comparison with the experiment, values for l_y, l_z, and l_x are taken from more realistic wave function calculations using an eight-band $\mathbf{k}\cdot\mathbf{p}$ model [44,45] and fitting the obtained electron and heavy-hole ground state probability densities with the density corresponding to the wave function from Eq. (1). The results are shown in Fig. 3. The obtained wave function extensions have been averaged arithmetically over electron and hole states (as no significant difference appeared between the dimensions obtained from the $\mathbf{k}\cdot\mathbf{p}$ calculations), which yields $\psi_n^{(e)}(\boldsymbol{r}) = \psi_n^{(h)}(\boldsymbol{r})$ in the model. For instance, a typical

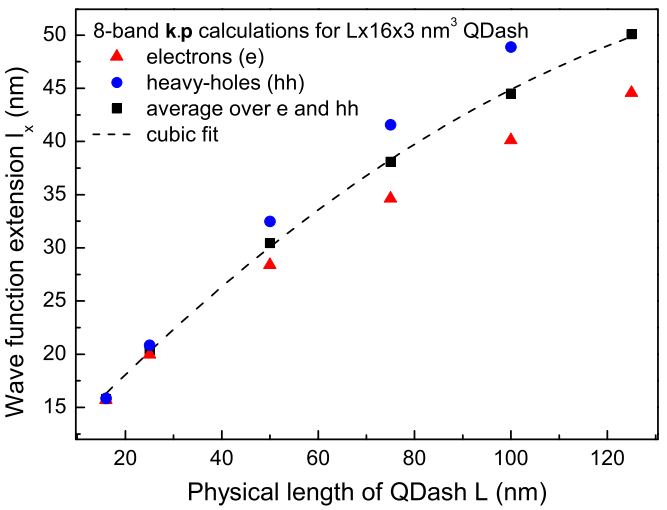

FIG. 3. (Color online) Wave-function localization length l_x dependence on the physical length of the QDash based on the eight-band $\mathbf{k}\cdot\mathbf{p}$ calculations.

QDash under consideration with its physical dimensions of $100 \times 16 \times 3.0\,\mathrm{nm}^3$ turns out to correspond to a wave function with the effective spatial extensions $l_x \times l_y \times l_z$ equal to $45 \times 5.3 \times 1.7\,\mathrm{nm}^3$. The scaling between the real size of the QDash and the wave-function extension for width and height occurred to be almost exactly linear with $l_y = D/3.0$ and $l_z = H/1.8$, while in the case of the length l_x it exhibits a weak cubic dependence (Fig. 3). Based on the single-particle wave functions one can construct the product basis for the excitonic states and diagonalize the Hamiltonian of the system, which has the form

$$H_0 = \sum_i E_i^{(e)} a_i^\dagger a_i + \sum_i E_i^{(h)} h_i^\dagger h_i + \sum_{ijkl} V_{ijkl} a_i^\dagger h_j^\dagger h_k a_l, \quad (2)$$

where $a_i^\dagger$, a_i and $h_i^\dagger$, h_i are electron and hole creation and annihilation operators, respectively. The first two terms describe the free carrier Hamiltonian, where $E_n^{(e/h)}$ are electron (hole) energies equal to

$$E_n^{(e/h)} = E_0^{(e/h)} + \frac{\hbar^2 \pi^2 n^2}{m_{e/h}^* 2 l_x^2},$$

expressed by the sum of the 2D harmonic oscillator ground state energy $E_0^{(e/h)}$ and the energy of quantized levels in a one-dimensional infinite well. The third term in Eq. (2) is the interaction part of the Hamiltonian, in which V_{ijkl} are the matrix elements of the electron-hole interaction

$$V_{ijkl} = -\int d^3 r_e \int d^3 r_h \psi_i^{(e)*}(\boldsymbol{r}_e)\psi_j^{(h)*}(\boldsymbol{r}_h) \times \left(\frac{e^2}{4\pi\varepsilon_s\varepsilon_0}\frac{1}{|\boldsymbol{r}_e - \boldsymbol{r}_h|}\right)\psi_k^{(h)}(\boldsymbol{r}_h)\psi_l^{(e)}(\boldsymbol{r}_e),$$

where ε_0 is the vacuum permittivity and ε_S is the static relative dielectric constant. Upon diagonalization of the Hamiltonian we derived the coefficients C_{nm} for the expansion of the exciton ground state $|X\rangle$ in the single particle states basis

$$|X\rangle = \sum_{ij} C_{ij} a_i^\dagger h_j^\dagger |0\rangle, \quad (3)$$

where $|0\rangle$ is the crystal ground state. This expression is then used for the calculations of phonon spectral densities and phonon-assisted exciton emission spectra as a function of temperature.

At this point, the coupling between electrons and acoustic phonons is included in the Hamiltonian of the system

$$H = H_0 + H_{\mathrm{ph}} + H_{\mathrm{int}},$$

where H_{ph} is the free phonon Hamiltonian

$$H_{\mathrm{ph}} = \sum_{\boldsymbol{k},s} \hbar\omega_{\boldsymbol{k},s} b_{\boldsymbol{k},s}^\dagger b_{\boldsymbol{k},s},$$

where $b_{\boldsymbol{k},s}^\dagger$, $b_{\boldsymbol{k},s}$ are creation and annihilation operators for a phonon in the mode s with the wave vector $\boldsymbol{k}$ and frequency $\omega_{\boldsymbol{k},s}$ ($s = l,t$ denotes the longitudinal and transverse acoustic phonon branches, respectively). The last term corresponds to the exciton-phonon interaction $H_{\mathrm{int}} = H_{\mathrm{int}}^{(e)} + H_{\mathrm{int}}^{(h)}$, with the electron part

$$H_{\mathrm{int}}^{(e)} = \sum_{nn',\boldsymbol{k},s} F_{nn',\boldsymbol{k},s}^{(e)} (b_{\boldsymbol{k},s}^\dagger + b_{-\boldsymbol{k},s}) a_n^\dagger a_{n'}$$

and analogous for holes, where $F_{nn',\boldsymbol{k},s} = F_{nn',-\boldsymbol{k},s}^*$ are the coupling constants. Since only long-wavelength phonons are effectively coupled to carriers confined in a QDash [32] we will always assume linear and isotropic dispersion for acoustic phonons $\omega_{k,s} = c_s k$, where c_s is the speed of sound. Since the exciton coupling with optical phonons is manifested in the emission by the presence of phonon replicas at energies $\hbar\Omega_0$ (36 meV for InAs) below the zero-phonon line [42], it does not contribute to the exciton line shape, and is thus neglected in our model.

In our study we are interested in the phonon sidebands that reflect phonon-assisted radiative recombination processes. We neglect the effect of real transitions between different exciton states, thus reducing our carrier-phonon coupling to the independent boson model [28–30], in which exciton states are only diagonally coupled to phonons, while phonon-induced transition terms are discarded. In fact, since only the ground exciton state contributes to the PL signal under the conditions of our experiment, only this state is relevant. Thus, the physics to be discussed is described by the Hamiltonian H_{int} projected on the ground exciton state, as defined in Eq. (3),

$$H_{\mathrm{int}}^{(X)} = \langle X|H_{\mathrm{int}}|X\rangle |X\rangle\langle X| = |X\rangle\langle X| \sum_{\boldsymbol{k},s} F_{\boldsymbol{k},s}^{(X)} (b_{\boldsymbol{k},s}^\dagger + b_{-\boldsymbol{k},s}),$$

where $F_{\boldsymbol{k},s}^{(X)}$ is the exciton-phonon coupling constant

$$F_{\boldsymbol{k},s}^{(X)} = \sum_{ijk} C_{ik}^* C_{jk} F_{ij,\boldsymbol{k},s}^{(e)} + \sum_{ijk} C_{ki}^* C_{kj} F_{ij,\boldsymbol{k},s}^{(h)},$$

$$F_{ij,\boldsymbol{k},s}^{(e/h)} = F_{ij,\boldsymbol{k}}^{(e/h)\mathrm{DP}} + F_{ij,\boldsymbol{k},s}^{(e/h)\mathrm{PE}}.$$

The electron and hole coupling includes the deformation potential (DP) and piezoelectric (PE) mechanisms with the respective coupling constants:

$$F_{nn',\boldsymbol{k}}^{(e/h)\mathrm{DP}} = \pm\sigma_{e/h}\sqrt{\frac{\hbar k}{2\rho V c_l}}\mathcal{F}_{nn'}^{(e/h)}(\boldsymbol{k}),$$

$$F_{nn',\boldsymbol{k},s}^{(e/h)\mathrm{PE}} = \mp i\sqrt{\frac{\hbar}{2\rho V c_s k}}\left(\frac{d_p e}{\varepsilon\varepsilon_0}\right) M_s(\hat{\boldsymbol{k}})\mathcal{F}_{nn'}^{(e/h)}(\boldsymbol{k}),$$

where ρ is the crystal density, V is the normalization volume of phonon modes, d_p is the piezoelectric constant, and $\mathcal{F}_{nn'}^{(e/h)}(\boldsymbol{k})$ is the form factor defined for electrons as

$$\mathcal{F}_{nn'}^{(e)}(\boldsymbol{k}) = \int d^3 r_e \psi_n^{(e)*}(\boldsymbol{r}_e) e^{i\boldsymbol{k}\cdot\boldsymbol{r}_e} \psi_{n'}^{(e)}(\boldsymbol{r}_e),$$

and analogously for holes. The function $M_s(\hat{\boldsymbol{k}})$ is a polarization-dependent geometrical factor (which depends only on phonon wave vector orientation),

$$M_s(\hat{\boldsymbol{k}}) = 2[\hat{k}_1\hat{k}_2(\hat{e}_{s,\hat{k}'})_3 + \hat{k}_2\hat{k}_3(\hat{e}_{s,\hat{k}'})_1 + \hat{k}_3\hat{k}_1(\hat{e}_{s,\hat{k}'})_2],$$

where $\hat{e}_{s,\hat{\boldsymbol{k}}'}$ is a unit polarization vector, and $\hat{\boldsymbol{k}}' = (\hat{k}_1,\hat{k}_2,\hat{k}_3)$ and $\hat{\boldsymbol{k}} = (\hat{k}_x,\hat{k}_y,\hat{k}_z)$ are wave vectors oriented along the crystallographic and QDash axis (elongation along the [1−10]

direction), respectively,

$$\hat{\boldsymbol{k}}' = \left(\frac{\hat{k}_x - \hat{k}_y}{\sqrt{2}}, \frac{\hat{k}_x + \hat{k}_y}{\sqrt{2}}, \hat{k}_z\right),$$

$$\hat{\boldsymbol{k}} = (\cos\theta, \sin\theta\cos\phi, \sin\theta\sin\phi).$$

We choose phonon polarizations $\hat{e}_{s,\hat{\boldsymbol{k}}'}$ as follows:

$$\hat{e}_{l,\hat{\boldsymbol{k}}'} = \boldsymbol{k}' = \left(\frac{\cos\theta - \sin\theta\cos\phi}{\sqrt{2}}, \frac{\cos\theta + \sin\theta\cos\phi}{\sqrt{2}}, \sin\theta\sin\phi\right),$$

$$\hat{e}_{t_1,\hat{\boldsymbol{k}}'} = \left(\frac{\sin\phi}{\sqrt{2}}, \frac{-\sin\theta}{\sqrt{2}}, \cos\phi\right),$$

$$\hat{e}_{t_2,\hat{\boldsymbol{k}}'} = \left(\frac{-\sin\theta - \cos\theta\cos\phi}{\sqrt{2}}, \frac{-\sin\theta + \cos\theta\cos\phi}{\sqrt{2}}, \cos\theta\sin\phi\right),$$

for which the functions $M_s(\hat{\boldsymbol{k}})$ read

$$M_l(\hat{\boldsymbol{k}}) = 3\sin\theta\sin\phi(\cos^2\theta - \sin^2\theta\cos^2\phi),$$

$$M_{t1}(\hat{\boldsymbol{k}}) = \cos\phi(3\sin^2\phi\sin^2\theta - 2\sin^2\theta + 1),$$

$$M_{t2}(\hat{\boldsymbol{k}}) = -\sin\phi\cos\theta(3\cos^2\phi\sin^2\theta + 2\sin^2\theta - \cos^2\theta).$$

The properties of the crystal lattice are characterized by the spectral densities, which we define in the temperature-dependent way,

$$\begin{aligned} R(\omega) &= \sum_{\boldsymbol{k},s} \left|\frac{F^{(X)}_{\boldsymbol{k},s}}{\hbar c_s k}\right|^2 [n_B(-\omega)\delta(\omega + c_s k) \\ &\quad + (n_B(\omega) + 1)\delta(\omega - c_s k)] \\ &= \frac{1}{(2\pi)^3}\sum_s \int d^3k \left|\frac{F^{(X)}_{\boldsymbol{k},s}}{\hbar c_s k}\right|^2 [n_B(-\omega)\delta(\omega + c_s k) \\ &\quad + (n_B(\omega) + 1)\delta(\omega - c_s k)], \end{aligned}$$

where $n_B(\omega)$ is Bose distribution function describing the influence of temperature on the phonon modes occupation.

Based on the standard results for the independent boson model [28–30], the emission spectrum for the spontaneous recombination of a confined exciton is expressed as

$$\tilde{f}(\omega) = e^{R_\infty}\delta(\omega) + \frac{1}{2\pi}e^{R_\infty}\int dt e^{i\omega t}[e^{\tilde{R}(t)} - 1],$$

where $R_\infty = -R(0)$, and $\tilde{R}(t)$ is the Fourier transform of $R(\omega)$. By introducing Gaussian profile of a central exciton line with the initial (low-temperature) width σ we get the inhomogenously broadened emission spectrum

$$\begin{aligned} f(\omega) &= \int d\omega' \frac{1}{\sigma\sqrt{2\pi}} e^{\frac{1}{2}\frac{(w-w')^2}{\sigma^2}} \tilde{f}(\omega'), \\ f(\omega) &= \frac{1}{\sqrt{2\pi}\sigma} e^{R_\infty - \frac{1}{2}\left(\frac{\omega^2}{\sigma^2}\right)} + \frac{1}{2\pi}\int dt e^{i\omega t} e^{-\frac{1}{2}\sigma^2 t^2}[e^{\tilde{R}(t)} - 1]. \end{aligned} \tag{4}$$

One has to notice that exciton-related emission line should in general have a Lorentzian-like shape. In an experiment, however, the spectral diffusion effects [42] lead to fluctuations of the exciton emission energy. This means that, when the time-integrated spectra are collected, a Gaussian profile is observed effectively, due to a much shorter time scale of these fluctuations in comparison to the typical data acquisition time. In our modeling we assume that this initial inhomogeneous broadening is primarily caused by spectral diffusion (SD), thus the initial linewidth (in the sense of a FWHM) will be later on denoted as σ^{SD} ($\sigma = \sigma^{\mathrm{SD}}/2\sqrt{2\ln 2}$). It should be mentioned also that we do not include the carrier losses with temperature, which is the main PL quenching mechanism observed in the experiment. This narrows the temperature range of the performed experiments down to 90–100 K.

C. Numerical results

In this section we present results of theoretical modeling of the exciton-acoustic-phonon coupling effect on the inhomogeneous emission line shape of a single exciton confined in a QDash. In order to point out how the geometry of a QDash influences the strength of the exciton-phonon coupling, the calculations have been performed for different QDash geometries, from symmetric objects resembling typical quantum dots up to strongly anisotropic structures with lateral aspect ratios larger than 5 corresponding to QDashes studied experimentally in this work.

In Fig. 4(a), calculated emission spectra for a typical InAs/InGaAlAs/InP QDash structure ($100 \times 16 \times 3\,\mathrm{nm}^3$) are presented in the 5–120 K temperature range. The initial width of the exciton line has been set to 0.1 meV, representing the typical broadening observed in the experiment. For clarity, the emission lines for different temperatures are shifted horizontally. One can clearly observe that with increasing temperature the lines become broader and start to differ significantly from the initial Gaussian profile, especially at

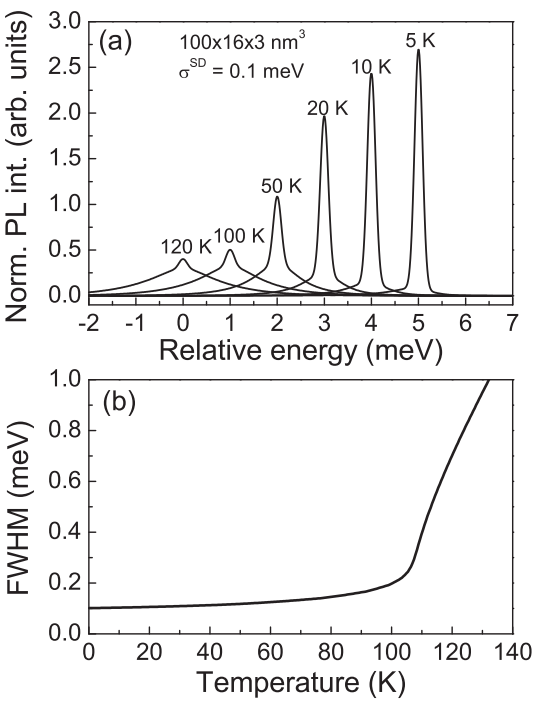

FIG. 4. (a) Calculated single exciton PL spectra of $100 \times 16 \times 3.0\,\mathrm{nm}^3$ InAs QDash, normalized to the integrated intensity for various temperatures with $\sigma^{\mathrm{SD}} = 0.1$ meV. For clarity, the energy positions of emission lines are shifted horizontally. (b) Temperature dependence of the full width at half maximum of the exciton line.

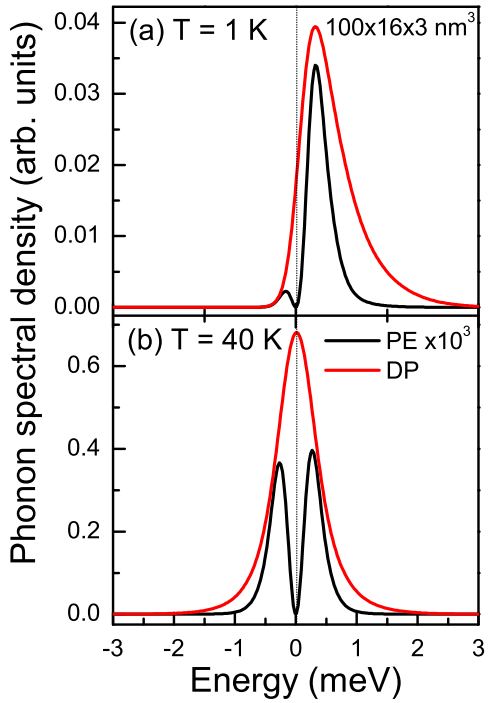

FIG. 5. (Color online) Calculated phonon spectral densities for a $100 \times 16 \times 3.0\,\mathrm{nm}^3$ InAs QDash at various temperatures, assuming exciton interaction with acoustic phonons via (a) deformation potential and (b) piezoelectric effect.

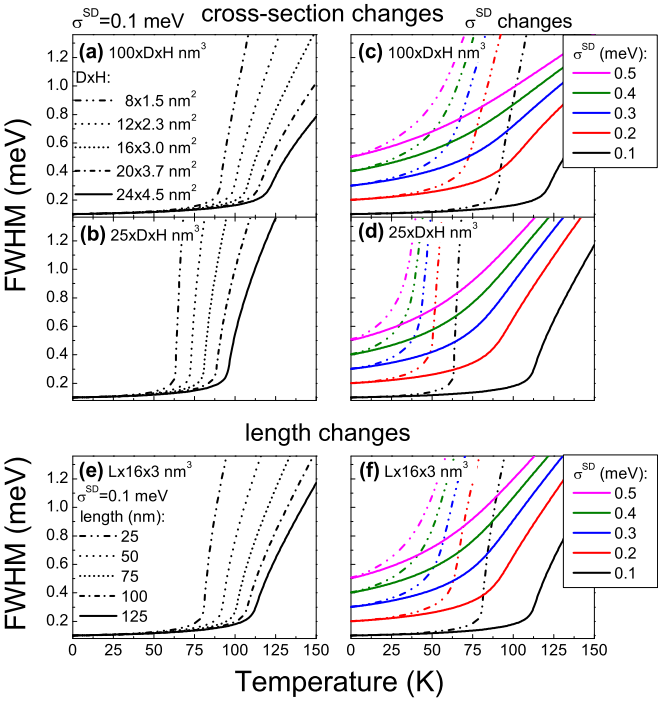

FIG. 6. (Color online) Calculated temperature dependence of the exciton emission line FWHM for two lengths of a QDash: (a) $L = 100$ nm and (b) $L = 25$ nm and a set of cross sections $D \times H$ ranging from 8×1.5 up to $24 \times 4.5\,\mathrm{nm}^2$. (c) and (d) Analogous dependencies of FWHM are presented for two extreme cross sections and σ^{SD} in the range of 0.1 to 0.5 meV. (e) Calculated temperature dependence of the exciton emission line FWHM of typical InAs QDashes with cross-section dimensions $D \times H = 16 \times 3.0\,\mathrm{nm}^2$ and a set of lengths L ranging from 25 to 125 nm. (f) Analogous dependencies of FWHM are presented for two extreme lengths and σ^{SD} in the range of 0.1 to 0.5 meV.

their bottom where the phonon-related sidebands start to appear (similarly as in Ref. [31]). At high temperatures (just above 100 K) the spectrum is already fully dominated by the phonon-assisted recombination. This tendency can be directly observed in the FWHM dependence on temperature shown in Fig. 4(b). The modeled curve is in a good qualitative agreement with experimental findings (see Fig. 2).

To compare the strength of different exciton-phonon coupling mechanisms, the phonon spectral densities have been calculated for DP (red lines) and PE (black lines) couplings independently (see Fig. 5). It turns out that the PE coupling is around 3 orders of magnitude weaker than the DP one for the investigated structures. In both cases the emission spectra are asymmetric at low temperatures, when the processes with the emission of phonons are favored with respect to those involving their absorption [see Fig. 5(a)]. In our experimental data, apparent asymmetry has also been observed for some lines but this is actually at the limit of the experimental accuracy and no trustworthy analysis or interpretation could be performed. When the temperature increases, the peak tends to symmetrize and for temperatures where the thermal energy $k_{\mathrm{B}}T$ becomes comparable or larger than the width of the phonon feature no asymmetry is observed [see Fig. 5(b) for $T = 40$ K], because both emission and absorption events have a similar probability.

Finally, we analyze the influence of the QDash geometry on the phonon-induced exciton decoherence. In Fig. 6 the temperature dependence of the exciton emission line FWHM for QDashes with cross-sectional dimensions ranging from 8×1.5 up to $24 \times 4.5\,\mathrm{nm}^2$ and two lengths (a) $L = 100$ nm and (b) $L = 25$ nm representing strongly anisotropic and almost symmetric in-plane objects, respectively, are presented. At low temperatures a slow and linear rise of FWHM up to 100–120 K for a 100 nm (75–100 K for 25 nm) long QDash can be observed. Above this critical temperature the FWHM increases rapidly. Both the slope of that increase as well as the critical temperature depend strongly on the cross-sectional dimension of the QDash ($D \times H$). An increase of $D \times H$, in general, suppresses the strength of the exciton interaction with phonons, shifts the critical temperature to higher values, and reduces the slope of the fast FWHM increase. Qualitatively, this attenuation effect is quite similar for both anisotropic and almost symmetric objects. In Figs. 6(c) and 6(d), analogous dependencies are presented for various low-temperature line broadenings governed by spectral diffusion effects, in the range of 0.1 to 0.5 meV. Increasing the σ^{SD} strongly changes the FWHM dependence on temperature. For low σ^{SD} two characteristic regimes can be distinguished, i.e., slow and fast increase of the FWHM. For larger σ^{SD} (FWHM > 0.3 meV), no such dependence is present and rather a smooth increase of the FWHM is observed instead. The elongation of a QDash does not change the picture qualitatively, however, the slope of the FWHM vs temperature curve gets less steep and the critical temperature shifts to larger values. This

behavior is even more pronounced in Figs. 6(e) and 6(f), where the temperature dependencies of exciton line FWHM are presented for various QDash lengths L ranging from 25 to 125 nm and $D \times H = 16 \times 3.0\,\mathrm{nm}^2$. When the QDash length is increased from 25 to 125 nm the critical temperature shifts from 80 to 115 K. Based on the presented results it can be predicted that indeed in the case of QDashes the influence of phonons should be strongly suppressed up to 100 K, but cannot be neglected at higher temperatures. As the main cause of that the nonlinear scaling of the wave-function extension in the elongation direction with the physical nanostructure dimensions has been identified. These considerations show the relative importance of the cross-sectional dimensions versus the QDash length due to much stronger confinement in these directions and, as a result, more significant wave-function sensitivity to the size changes.

D. Comparison with the experiment

In Fig. 7 a direct comparison of the theoretical and experimental temperature dependence of FWHM is shown for four excitonic lines coming from different dashes of the same sample. To fit the experimental data, nominal sizes for the cross section ($16 \times 3.0\,\mathrm{nm}^2$) as well as the value of spectral diffusion (taken from low-temperature FWHM of the respective spectral lines) have been fixed and only the dash length L was varied. In Figs. 7(c) and 7(d) the best agreement can indeed be seen for the lengths close to the nominal 100 nm, suggesting that these lines represent the excitonic emission from extended states of typical anisotropic objects. In the case of lines shown in Figs. 7(a) and 7(b) the lengths had to be reduced down to even 20 nm in order to get good matching of the calculated curve to the experimental data. These two lines may be attributed to the excitons confined in a much smaller volume than the nominal 100 nm. This, in case of our structures, corresponds most probably to the existence of a localization center within the certain dash. These observations are in qualitative agreement with our previous studies on the ensemble of dashes, which predicted the coexistence of the two types of confinement regimes in these nanostructures. Additionally, they correlate well with the results of time-resolved experiments [24] performed on the same single emission lines, since in the case of QDash excitons corresponding to Figs. 7(a) and 7(b) the decay times are much shorter (1.4–1.7 ns) than for the case of Figs. 7(c) and 7(d) (approximately 2.1 ns), suggesting indeed substantial differences in the confining potential. Similarly, the initial broadenings at low temperatures differ significantly between those two groups of lines (0.08–0.14 versus 0.18–0.25 meV) which may be a fingerprint of a different exciton electric polarizability, which should vary depending on the effective confining potential volume: a larger *e-h* separation expected for larger objects causes a stronger effect of the local electric field fluctuations.

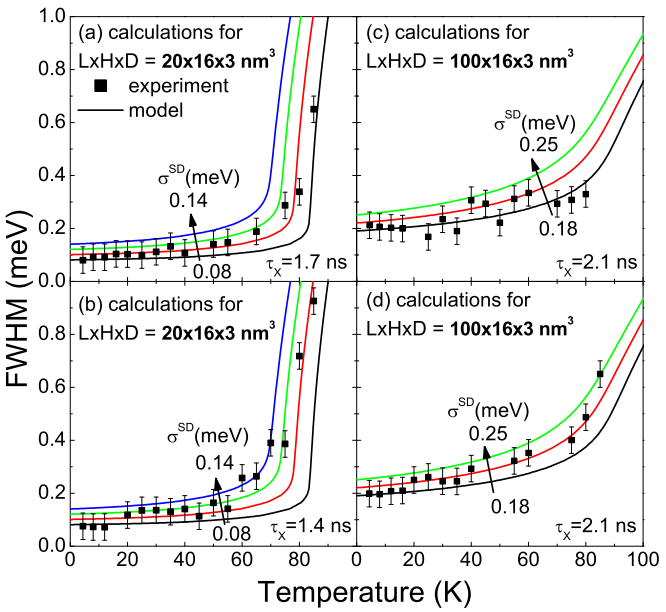

FIG. 7. (Color online) Temperature dependence for the four exciton PL emission lines FWHM. Black squares represent experimental data obtained for QDashes originating from the sample with nominal dashes size of $100 \times 16 \times 3.0\,\mathrm{nm}^3$. Color solid lines are modeled curves for fixed values of $D \times H = 16 \times 3.0\,\mathrm{nm}^3$ and lengths L equal to 20 nm in the case of (a) and (b) and 100 nm in the case of (c) and (d). Different colors represent different values of σ^{SD} in the ranges 0.08–0.14 and 0.18–0.25 meV for (a), (b) and (c), (d), respectively. Decay times τ_D are determined from time-resolved experiments performed as in Ref. [24].

IV. SUMMARY

We have studied, both theoretically and experimentally, the phonon-assisted recombination process of excitons confined in strongly anisotropic epitaxial nanostructures for the example of InAs/InGaAlAs/InP semiconductor quantum dashes. Within the independent boson model we have found that acoustic phonons couple to the exciton almost exclusively via the deformation potential mechanism, so that the piezoelectric contribution is negligible. Our analysis has revealed that the influence of the QDash geometry on the exciton-phonon interaction is determined by the wave-function extension and confirmed that indeed for strongly elongated nanostructures the influence of phonon-related decoherence is expected to be significantly weaker in comparison to typical QDs, but cannot be entirely neglected and dominates the emission spectra above 100 K. For a proper interpretation of the experimental data a correspondence between the wave-function extension and the physical dimension needed to be found for such large objects. It showed the crucial role of the cross-sectional dimensions and slightly weaker impact of the length for the range of realistic physical sizes of the dashes. The theoretical predictions have been supported by the experiment and quite a good qualitative agreement has been obtained. Two types of confinement regimes for the QDash excitons have been revealed: one for which the wave function is extended over the whole QDash volume, and second, with wave-function extension much smaller than expected based on the nominal QDash dimensions. This observation has been interpreted in terms of exciton localization, which decreases the object physical anisotropy and the effective exciton coherence volume, in

agreement with our previous preliminary predictions. In this report experimental evidence of this dual character of the system ground state for individual QDashes is presented. The possibility to distinguish between these two types of states opens up new opportunities to study in detail the influence of the confinement regime. These results can be helpful in designing novel nanostructures that could emit light with strongly reduced contribution of phonon-assisted processes, which is crucial for all the modern information processing schemes.

ACKNOWLEDGMENTS

The work has partly been realized within Grant No. 2011/02/A/ST3/00152 of the National Science Centre of Poland. The experiments have partially been performed within the laboratory infrastructure financed by the Polish Ministry of Science and Higher Education Grant No. 6167/IA/119/2012. J.M. acknowledges the financial support from COPERNICUS Award of the Foundation for Polish Science (FNP) and Deutsche Forschungsgemeinschaft (DFG). The fellowship co-financed by the European Commission within European Social Fund is also acknowledged.

[1] S. P. Guo, H. Ohno, A. Shen, F. Matsukura, and Y. Ohno, Appl. Phys. Lett. **70**, 2738 (1997).
[2] J. Brault, M. Gendry, G. Grenet, G. Hollinger, Y. Desiéres, and T. Benyattou, Appl. Phys. Lett. **73**, 2932 (1998).
[3] J. M. Garcia, L. Gonzales, M. U. Gonzalez, J. P. Silveira, Y. Gonzalez, and F. Briones, J. Cryst. Growth **227**, 975 (2001).
[4] A. Sauerwald, T. Kümmell, G. Bacher, A. Somers, R. Schwertberger, J. P. Reithmaier, and A. Forchel, Appl. Phys. Lett. **86**, 253112 (2005).
[5] R. Schwertberger, D. Gold, J. P. Reithmaier, and A. Forchel, IEEE Photon Technol. Lett. **14**, 735 (2002).
[6] M. Jo, T. Mano, and K. Sakoda, Appl. Phys. Express **3**, 045502 (2010).
[7] T. Utzmeier, P. A. Postigo, J. Tamayo, R. García, and F. Briones, Appl. Phys. Lett. **69**, 2674 (1996).
[8] N. Sritirawisarn, F. W. M. van Otten, T. J. Eijkemans, and R. Nötzel, J. Appl. Phys. **102**, 053514 (2007).
[9] J. P. Reithmaier, G. Eisenstein, and A. Forchel, Proc. IEEE **95**, 1779 (2007).
[10] J. P. Reithmaier, A. Somers, S. Deubert, R. Schwertberger, W. Kaiser, A. Forchel, M. Calligaro, P. Resneau, O. Parillaud, S. Bansropun, M. Krakowski, R. Alizon, D. Hadass, A. Bilenca, H. Dery, V. Mikhelashvili, G. Eisenstain, M. Gioannini, I. Montrosset, T. W. Berg, M. van der Poel, J. Mork, and B. Tromborg, J. Phys. D: Appl. Phys. **38**, 2088 (2005).
[11] F. Lelarge, B. Dagens, J. Renaudier, R. Brenot, A. Accard, F. van Dijk, D. Make, O. Le Gouezigou, J.-G. Provost, F. Poingt, J. Landreau, O. Drisse, E. Derouin, B. Rousseau, F. Pommereau, and G.-H. Duan, J. Sel. Top. Quantum Electron. **13**, 111 (2007).
[12] A. Capua, G. Eisenstein, and J. P. Reithmaier, Appl. Phys. Lett. **97**, 131108 (2010).
[13] D. Hadass, R. Alizon, H. Dery, V. Mikhelashvili, G. Eisenstein, R. Schwertberger, A. Somers, J. P. Reithmaier, A. Forchel, M. Calligaro, S. Bansropun, and M. Krakowski, Appl. Phys. Lett. **85**, 5505 (2004).
[14] N. A. Jahan, C. Hermannstädter, J.-H. Huh, H. Sasakura, T. J. Rotter, P. Ahirwar, G. Balakrishnan, K. Akahane, M. Sasaki, H. Kumano, and I. Suemune, J. Appl. Phys. **113**, 033506 (2013).
[15] G. Sęk, M. Motyka, K. Ryczko, J. Andrzejewski, R. Kudrawiec, J. Misiewicz, F. Lelarge, B. Rousseau, and G. Patriarche, Proc. SPIE 6481, Quantum Dots, Particles, and Nanoclusters IV, 64810D (2007).
[16] A. A. Ukhanov, R. H. Wang, T. J. Rotter, A. Stintz, L. F. Lester, P. G. Eliseev, and K. J. Malloy, Appl. Phys. Lett. **81**, 981 (2002).
[17] M. Syperek, Ł. Dusanowski, J. Andrzejewski, W. Rudno-Rudziński, G. Sęk, J. Misiewicz, and F. Lelarge, Appl. Phys. Lett. **103**, 083104 (2013).
[18] T. Mensing, L. Worschech, R. Schwertberger, J. P. Reithmaier, and A. Forchel, Appl. Phys. Lett. **82**, 2799 (2003).
[19] N. Chauvin, B. Salem, G. Bremond, G. Guillot, C. Bru-Chevallier, and M. Gendry, J. Appl. Phys. **100**, 073702 (2006).
[20] N. Chauvin, G. Bremond, C. Bru-Chevallier, E. Dupuy, P. Regreny, and M. Gendry, Phys. Status Solidi C **3**, 3912 (2006).
[21] N. Chauvin, P. Nedel, C. Seassal, B. Ben Bakir, X. Letartre, M. Gendry, A. Fiore, and P. Viktorovitch, Phys. Rev. B **80**, 045315 (2009).
[22] G. Sęk, P. Podemski, A. Musiał, J. Misiewicz, S. Hein, S. Höffling, and A. Forchel, J. Appl. Phys. **105**, 086104 (2009).
[23] P. Mrowiński, A. Musiał, G. Sęk, J. Misiewicz, S. Höfling, A. Somers, S. Hein, and A. Forchel, Acta Phys. Pol. A **124**, 801 (2013).
[24] Ł. Dusanowski, M. Syperek, W. Rudno-Rudziński, P. Mrowiński, G. Sęk, J. Misiewicz, A. Somers, J. P. Reithmaier, S. Höfling, and A. Forchel, Appl. Phys. Lett. **103**, 253113 (2013).
[25] P. Kaczmarkiewicz and P. Machnikowski, Semicond. Sci. Technol. **27**, 105012 (2012).
[26] A. Musiał, P. Kaczmarkiewicz, G. Sęk, P. Podemski, P. Machnikowski, J. Misiewicz, S. Hein, S. Höfling, and A. Forchel, Phys. Rev. B **85**, 035314 (2012).
[27] E. Peter, J. Hours, P. Senellart, A. Vasanelli, A. Cavanna, J. Bloch, and J. M. Gérard, Phys. Rev. B **69**, 041307(R) (2004).
[28] K. Huang and A. Rhys, Proc. R. Soc. London Sect. A **204**, 406 (1950).
[29] C. B. Duke and G. D. Mahan, Phys. Rev. **139**, A1965 (1965).
[30] G. D. Mahan, *Many-Particle Physics* (Plenum, New York, 1990).
[31] L. Besombes, K. Kheng, L. Marsal, H. Mariette, Phys. Rev. B **63**, 155307 (2001).
[32] A. Grodecka, L. Jacak, P. Machnikowski, and K. Roszak, in *Quantum Dots: Research Developments*, edited by P. A. Ling (Nova Science, New York, 2005), p. 47.
[33] M. Bayer and A. Forchel, Phys. Rev. B **65**, 041308(R) (2002).

[34] P. Borri, W. Langbein, U. Woggon, V. Stavarache, D. Reuter, and A. D. Wieck, Phys. Rev. B **71**, 115328 (2005).
[35] E. Peter, P. Senellart, D. Martrou, A. Lemaitre, J. Hours, J. M. Gérard, and J. Bloch, Phys. Rev. Lett. **95**, 067401 (2005).
[36] B. Krummheuer, V. M. Axt, and T. Kuhn, Phys. Rev. B **65**, 195313 (2002).
[37] A. Vagov, V. M. Axt, T. Kuhn, W. Langbein, P. Borri, and U. Woggon, Phys. Rev. B **70**, 201305 (2004).
[38] P. Borri, W. Langbein, S. Schneider, U. Woggon, R. L. Sellin, D. Ouyang, and D. Bimberg, Phys. Rev. Lett. **87**, 157401 (2001).
[39] J. P. Reithmaier and A. Forchel, IEEE J. Sel. Top. Quantum Electron. **8**, 1035 (2002).
[40] T. Miyazawa, K. Takemoto, Y. Sakuma, S. Hirose, T. Usuki, N. Yokoyama, M. Takatsu, and Y. Arakawa, Jpn. J. Appl. Phys. **44**, L620 (2005).
[41] P. Kaczmarkiewicz, A. Musiał, G. Sęk, P. Podemski, P. Machnikowski, and J. Misiewicz, Acta Phys. Pol. A **119**, 633 (2011).
[42] J. Seufert, R. Weigand, G. Bacher, T. Kümmell, A. Forchel, K. Leonardi, and D. Hommel, Appl. Phys. Lett. **76**, 1872 (2000).
[43] G. W. Wen, J. Y. Lin, H. X. Jiang, and Z. Chen, Phys. Rev. B **52**, 5913 (1995).
[44] J. Andrzejewski, G. Sęk, E. O'Reilly, A. Fiore, and J. Misiewicz, J. Appl. Phys. **107**, 073509 (2010).
[45] J. Andrzejewski, J. Comput. Phys. **249**, 22 (2013).